Proceedings of the XII International Symposium on Dynamic Problems of Mechanics (DINAME 2007),
Varoto, P. S. and Trindade, M. A. (Editors), ABCM, Ilhabela, SP, Brazil, February 26 - March 2, 2007

Theoretical model results of rub in real rotating machinery

Nicolò Bachschmid, Paolo Pennacchi

Dept. of Mechanics, Politecnico di Milano, Via La Masa 34, I-20156 Milan, Italy, nicolo.bachschmid@polimi.it, paolo.pennacchi@polimi.it

Abstract: The occurrence of full annular rub or partial rub conditions in turbomachinery employed in power plants has become frequent due to the reduced clearances used to improve the efficiency in new design machines. This fact has stimulated the study of rotor-to stator rub phenomena. Some aspects have been already analyzed by the authors, which in the past developed a rather sophisticated model to simulate and reproduce the phenomenon of "spiral vibrations" or thermally excited vibrations. This paper analyzes rubs of short duration, which can occur for instance when the shaft is passing a critical speed during the coast down transient and which are not able to induce consistent thermal bows and the associated spiral vibrations, but should also be identified by suitable measurements. From literature it is known that these phenomena can be identified by means of vibration measurements on the stator of the machine as well as by the associated emitted noise. The friction forces affect also the rotating speed of the shaft: the accurate measurement of the speed and of its harmonic components could also allow to identify a rubbing condition. These aspects are investigated by means of a model of the MODAROT test-rig which had been modified to allow rub conditions to occur. A model of the partial arc rub condition has also been set, in order to verify the effects of the rub on the vibrations, and on the rotating speed. The behaviour of the model is analysed in the time domain, due to the non-linearity of the phenomenon.

Keywords: Rotor-to-stator rub, rotor dynamics, contacts, friction.

INTRODUCTION

Rubbing phenomena can occur frequently in rotating machinery, especially when clearances are tight and problems in alignment conditions between rotating part and stationary parts of the machine have shown. This can occur in the start up procedures of a new machine or of an older machine after an overhaul. The problem can also occur due to a thermal bow of the shaft, or to a thermal distortion of the stationary casing.

The contact can occur in one point only of the stationary part and the contact point is sliding on the surface of the shaft. This contact may be continuous or intermittent (also with rebounds) depending on stiffness and damping of both rotating and stationary part, and on the size and shape of unbounded orbit as imposed by unbalance and bow of the shaft.

The contact can also occur in one point only of the shaft which is then sliding on one arc (partial arc rub) or on the complete circumference of the casing (full annular rub). In this case the friction effects a local heating on the shaft, the shaft gets a thermal bow, and stable or unstable spiral vibrations are excited.

Many of the physical phenomena which occur during rotor to stator rub have been described firstly in a literature survey of Muszynska (1989). If the contact is continuous and a full annular rub is generated, the friction force may excite a very dangerous dry friction reverse whirl in smaller machines. If the contact is occasional and associated to rebounds, also chaotic motion can result in light shafts. During the contact, the stiffness "felt" by the rubbing shaft is higher than the flexural stiffness of the shaft: during one rotation the shaft experiences a non-linear stiffness and has consequently the typical behaviour of a vibrating system with non-linear stiffness. All these phenomena have never been measured on big sized industrial machines like steam turbines and generators, which are the main objects of the present analysis on rubbing rotors.

Spiral vibrations have been extensively analysed by means of suitable models both for the thermal behaviour and for the consequent vibration behaviour in Bachschmid et al. (2000) and Bachschmid et al. (2004).

In recent years when the requirement of higher efficiency in turbo-machinery has reduced the clearances between rotating shafts, impellers and blade rows and stationary parts, the analysis of rubbing rotors has become a matter of great interest.

From a diagnostic point of view it is necessary to recognize rubs from few measurements. Spiral vibrations constitute a strong symptom of full annular or partial arc rub, but sometimes also spiral vibrations were attributed to other causes (whirling motion in oil-film bearings). Intermittent rubs are more difficult to be recognized, because apparently they affect only lightly the vibrations of the casing introducing some high frequency noise, which could be detected by accelerometers or also by acoustic measurements Stagemann et al. (1993).

A theoretical and experimental research has been started in order to analyse the dynamical behaviour of a shaft rubbing against a partial seal ring: the contact occurs in one point only of the stationary part (the seal ring) and is

intermittent. A test rig with a shaft on two oil-film bearings has been modified to allow different measurements in rubbing conditions.

Firstly a theoretical investigation has been started for analysing all possible symptoms of a rotating shaft, which is brought in contact with an obstacle, which is also a vibrating system, equipped with a partial arc seal ring. In the present paper the main results of this investigation are presented. For the simulations the model of the test rig has been used, the rotor is represented by a f.e.m. with 5 degrees of freedom per node (to include also torsional vibrations), the obstacle is a 6 d.o.f. system with a spring representing the seal ring, the normal contact force is calculated considering the (linear) stiffness of the seal ring spring and its deflection, when the shaft orbit exceeds the clearance. The tangential friction force is calculated considering the friction coefficient times the normal contact force. The friction force excites both flexural and torsional vibrations. Orbits in bearings and in correspondence of the seal ring are calculated with and without rub integrating the equations in the time domain. Also vibrations of the obstacle, contact force and torsional vibrations are calculated each time step.

DESCRIPTION OF THE MODEL

In this section the complete model of the system is described, even some simplification in regards to the supporting structure will be actually introduced in the following. The rotor is modelled by means of finite beam elements, taking also into account the shear and the secondary effect of rotatory inertia. Due to the fact that not only the lateral response but also the torsional vibration will be considered, 5 d.o.f.s (two translational and three rotational) are considered per each node. Axial vibrations will be neglected. The generalized displacement vector $\mathbf{x}_j^{(r)}$ of the rotor *j*-th node is:

$$\mathbf{x}_j^{(r)} = \left\{ x_j^{(r)} \quad y_j^{(r)} \quad \vartheta_{x_j}^{(r)} \quad \vartheta_{y_j}^{(r)} \quad \vartheta_{z_j}^{(r)} \right\}^{\mathrm{T}} \tag{1}$$

Two subsequent nodes, the *j*-th and the *j*+1-th, define the *j*-th element of the machine as shown in figure 1 along with the reference system on the rotor. If the rotor has n_r nodes, thus $n_r - 1$ elements, the vector $\mathbf{x}^{(r)}$ of the generalized displacements of all the rotor nodes is composed by all the ordered vectors $\mathbf{x}_j^{(r)}$ as shown in eq. (2):

$$\mathbf{x}^{(r)} = \left\{ x_1^{(r)} \quad y_1^{(r)} \quad \vartheta_{x_1}^{(r)} \quad \vartheta_{y_1}^{(r)} \quad \vartheta_{z_1}^{(r)} \cdots x_{n_r}^{(r)} \quad y_{n_r}^{(r)} \quad \vartheta_{x_{n_r}}^{(r)} \quad \vartheta_{y_{n_r}}^{(r)} \quad \vartheta_{z_{n_r}}^{(r)} \right\}^{\mathrm{T}} \tag{2}$$

Different methods can be used to model the foundation. For the sake of brevity, only pedestals, i.e. lumped 2 d.o.f.s systems, will be considered. A discussion about other methods is reported in Pennacchi et al. (2006). In a similar manner to the rotor, also the d.o.f.s of the foundation, horizontal and vertical displacements, which are connected by the n_b bearings to the rotor, can be ordered in a vector:

$$\mathbf{x}^{(f)} = \left\{ x_1^{(f)} \quad y_1^{(f)} \cdots x_{n_b}^{(f)} \quad y_{n_b}^{(f)} \right\}^{\mathrm{T}} \tag{3}$$

Finally, the housing of the seal strip and its housing will be considered as the rigid body P (see Figure 2) that has 6 d.o.f.s:

$$\mathbf{x}_{\mathrm{P}} = \left\{ x_{\mathrm{P}} \quad y_{\mathrm{P}} \quad z_{\mathrm{P}} \quad \vartheta_{x_{\mathrm{P}}} \quad \vartheta_{y_{\mathrm{P}}} \quad \vartheta_{z_{\mathrm{P}}} \right\}^{\mathrm{T}} \tag{4}$$

The complete vector of the generalized displacements of the model is therefore:

$$\mathbf{x} = \left\{ \mathbf{x}^{(r)} \quad \mathbf{x}^{(f)} \quad \mathbf{x}_{\mathrm{P}} \right\}^{\mathrm{T}} \tag{5}$$

Using Lagrange's method and neglecting the effect of external forces and of the rub, the d.o.f.s of the rotor, of the foundation and of the housing can be considered separately:

$$\begin{aligned} &\frac{d}{dt}\left(\frac{\partial T}{\partial \dot{x}^{(r)}}\right) - \frac{\partial T}{\partial x^{(r)}} + \frac{\partial U}{\partial x^{(r)}} = \frac{\delta W}{\delta x^{(r)}} \rightarrow \\ &\left[\mathbf{M}^{(r)}\right]\ddot{\mathbf{x}}^{(r)} + \left(\left[\mathbf{C}^{(r)}\right] + \Omega\left[\mathbf{G}^{(r)}\right]\right)\dot{\mathbf{x}}^{(r)} + \left[\mathbf{K}^{(r)}\right]\mathbf{x}^{(r)} = \frac{\delta W}{\delta x^{(r)}} \end{aligned} \tag{6}$$

$$\frac{d}{dt}\left(\frac{\partial T}{\partial \dot{x}^{(f)}}\right) - \frac{\partial T}{\partial x^{(f)}} + \frac{\partial U}{\partial x^{(f)}} = \frac{\delta W}{\delta x^{(f)}} \rightarrow \left[\mathbf{M}^{(f)}\right]\ddot{\mathbf{x}}^{(f)} + \left[\mathbf{C}^{(f)}\right]\dot{\mathbf{x}}^{(f)} + \left[\mathbf{K}^{(f)}\right]\mathbf{x}^{(f)} = \frac{\delta W}{\delta x^{(f)}} \tag{7}$$

$$\frac{d}{dt}\left(\frac{\partial T}{\partial \dot{x}_{\mathrm{P}}}\right)-\frac{\partial T}{\partial x_{\mathrm{P}}}+\frac{\partial U}{\partial x_{\mathrm{P}}}=\frac{\delta W}{\delta x_{\mathrm{P}}}\rightarrow[\mathbf{M}_{\mathrm{P}}]\ddot{\mathbf{x}}_{\mathrm{P}}+[\mathbf{C}_{\mathrm{P}}]\dot{\mathbf{x}}_{\mathrm{P}}+[\mathbf{K}_{\mathrm{P}}]\mathbf{x}_{\mathrm{P}}=\frac{\delta W}{\delta x_{\mathrm{P}}} \tag{8}$$

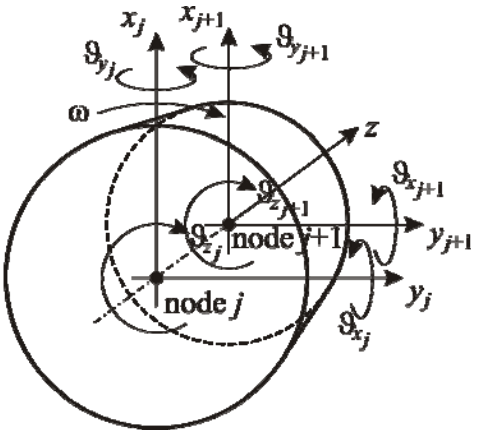

Figure 1. Reference systems of a general rotor element.

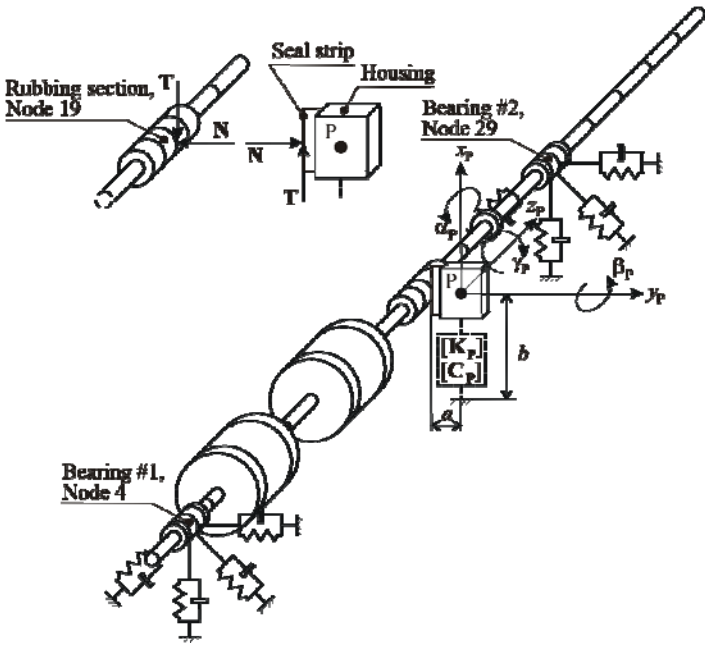

Figure 2. General layout of the test-rig.

In regards to the rotor, the mass matrix $[\mathbf{M}^{(r)}]$, which takes also into account the secondary effect of the rotatory inertia, the internal damping matrix $[\mathbf{C}^{(r)}]$, the stiffness matrix $[\mathbf{K}^{(r)}]$, which takes also into account the shear effect, and the gyroscopic matrix $[\mathbf{G}^{(r)}]$, all of order $(5n_r \times 5n_r)$, can be defined by means of standard Lagrange's methods, beam elements and lumped disks as shown e.g. in Lalanne and Ferraris (1998) and Childs (1993). Whilst the structure of $[\mathbf{M}^{(f)}]$, $[\mathbf{C}^{(f)}]$ and $[\mathbf{K}^{(f)}]$ is not relevant at this stage and depends on how the pedestals are implemented, the matrices of the housing are all simply diagonal matrices:

$$[\mathbf{M}_{\mathrm{P}}]=\mathrm{diag}(m_{\mathrm{P}},m_{\mathrm{P}},m_{\mathrm{P}},I_{\mathrm{P}_x},I_{\mathrm{P}_y},I_{\mathrm{P}_z}) \tag{9}$$

$$[\mathbf{C}_{\mathrm{P}}]=\mathrm{diag}(c_{\mathrm{P}_x},c_{\mathrm{P}_y},c_{\mathrm{P}_z},c_{t\mathrm{P}_x},c_{t\mathrm{P}_y},c_{t\mathrm{P}_z}) \tag{10}$$

$$[\mathbf{K}_{\mathrm{P}}]=\mathrm{diag}(k_{\mathrm{P}_x},k_{\mathrm{P}_y},k_{\mathrm{P}_z},k_{t\mathrm{P}_x},k_{t\mathrm{P}_y},k_{t\mathrm{P}_z}) \tag{11}$$

In order to consider the r.h.s of eqs. (6) and (7), the test-rig rotor is supported by n_b oil-film bearings that realize a coupling between the rotor and the supporting structure. Even if the exact calculation of the forces exchanged between the journal and the bearing case, due to the oil-film, requires appropriate methods, the discussion of which is far from the scope of present paper, a widely accepted simplification in rotor-dynamics simulation (see again Lalanne and Ferraris (1998) and Childs (1993)) is the modelling of the oil-film force field by means of linearized stiffness and damping coefficients function of the rotating speed. Therefore, the expression of the linearized forces of the oil-film of the *i*-th bearing on the rotor journal located in the *j*-th node, due to the rotor d.o.f. displacements only, is:

$$\begin{aligned}\mathbf{F}_i^{(br)}(\Omega)&=-\begin{bmatrix}k_{xx_i}^{(b)}(\Omega) & k_{xy_i}^{(b)}(\Omega) & 0 & 0 & 0\\ k_{yx_i}^{(b)}(\Omega) & k_{yy_i}^{(b)}(\Omega) & 0 & 0 & 0\\ 0 & 0 & 0 & 0 & 0\\ 0 & 0 & 0 & 0 & 0\\ 0 & 0 & 0 & 0 & 0\end{bmatrix}\begin{Bmatrix}x_j^{(r)}\\ y_j^{(r)}\\ \vartheta_{x_j}^{(r)}\\ \vartheta_{y_j}^{(r)}\\ \vartheta_{z_j}^{(r)}\end{Bmatrix}-\begin{bmatrix}r_{xx_i}^{(b)}(\Omega) & r_{xy_i}^{(b)}(\Omega) & 0 & 0 & 0\\ r_{yx_i}^{(b)}(\Omega) & r_{yy_i}^{(b)}(\Omega) & 0 & 0 & 0\\ 0 & 0 & 0 & 0 & 0\\ 0 & 0 & 0 & 0 & 0\\ 0 & 0 & 0 & 0 & 0\end{bmatrix}\begin{Bmatrix}\dot{x}_j^{(r)}\\ \dot{y}_j^{(r)}\\ \dot{\vartheta}_{x_j}^{(r)}\\ \dot{\vartheta}_{y_j}^{(r)}\\ \dot{\vartheta}_{z_j}^{(r)}\end{Bmatrix}=\\ &=-\left[\mathbf{K}_i^{(b)}(\Omega)\right]\mathbf{x}_j^{(r)}-\left[\mathbf{C}_i^{(b)}(\Omega)\right]\dot{\mathbf{x}}_j^{(r)}\end{aligned} \tag{12}$$

while that of the forces on the supporting structure, corresponding to the *i*-th bearing and due to the foundation d.o.f. only, is:

$$\begin{aligned}\mathbf{F}_i^{(bf)}(\Omega) &= -\begin{bmatrix} k_{xx_i}^{(b)}(\Omega) & k_{xy_i}^{(b)}(\Omega) \\ k_{yx_i}^{(b)}(\Omega) & k_{yy_i}^{(b)}(\Omega) \end{bmatrix} \begin{Bmatrix} x_j^{(f)} \\ y_j^{(f)} \end{Bmatrix} - \begin{bmatrix} r_{xx_i}^{(b)}(\Omega) & r_{xy_i}^{(b)}(\Omega) \\ r_{yx_i}^{(b)}(\Omega) & r_{yy_i}^{(b)}(\Omega) \end{bmatrix} \begin{Bmatrix} \dot{x}_j^{(f)} \\ \dot{y}_j^{(f)} \end{Bmatrix} = \\ &= -\left[\widehat{\mathbf{K}}_i^{(b)}(\Omega)\right]\mathbf{x}_j^{(f)} - \left[\widehat{\mathbf{C}}_i^{(b)}(\Omega)\right]\dot{\mathbf{x}}_j^{(f)}\end{aligned} \tag{13}$$

The actual bearing force between the rotor and the foundation is given by the difference between eq. (12) and eq. (13). This way the coupling effect of the oil-film forces is taken into account by the relative displacements of the nodes of the rotor and of the foundation in correspondence of the bearings and the fully assembled system of equation is built up.

This requires the definition of the stiffness coupling matrices $[\mathbf{K}^{(rr)}]$, $[\mathbf{K}^{(rf)}]$, $[\mathbf{K}^{(fr)}]$, $[\mathbf{K}^{(ff)}]$ and the corresponding damping matrices $[\mathbf{C}^{(rr)}]$, $[\mathbf{C}^{(rf)}]$, $[\mathbf{C}^{(fr)}]$, $[\mathbf{C}^{(ff)}]$, which are sparse and respectively of order $(5n_r \times 5n_r)$, $(5n_r \times 2n_b)$, $(2n_b \times 5n_r)$ and $(2n_b \times 2n_b)$. The structure for the stiffness matrices is:

$$[\mathbf{K}^{(rr)}] = \mathrm{diag}\left(\cdots \quad \left[\mathbf{K}_i^{(b)}(\Omega)\right] \quad \cdots\right) \tag{14}$$

$$[\mathbf{K}^{(fr)}] = \begin{bmatrix} \cdots & \cdots & \cdots & \cdots & \cdots & \cdots & \cdots \\ \cdots & k_{xx_i}^{(b)}(\Omega) & k_{xy_i}^{(b)}(\Omega) & 0 & 0 & 0 & \cdots \\ \cdots & k_{yx_i}^{(b)}(\Omega) & k_{yy_i}^{(b)}(\Omega) & 0 & 0 & 0 & \cdots \\ \cdots & \cdots & \cdots & \cdots & \cdots & \cdots & \cdots \end{bmatrix} \tag{15}$$

$$[\mathbf{K}^{(rf)}] = \begin{bmatrix} \cdots & \cdots & \cdots & \cdots \\ \cdots & k_{xx_i}^{(b)}(\Omega) & k_{xy_i}^{(b)}(\Omega) & \cdots \\ \cdots & k_{yx_i}^{(b)}(\Omega) & k_{yy_i}^{(b)}(\Omega) & \cdots \\ \cdots & 0 & 0 & \cdots \\ \cdots & 0 & 0 & \cdots \\ \cdots & 0 & 0 & \cdots \\ \cdots & \cdots & \cdots & \cdots \end{bmatrix} \tag{16}$$

$$[\mathbf{K}^{(ff)}] = \mathrm{diag}\left(\cdots \quad \left[\widehat{\mathbf{K}}_i^{(b)}(\Omega)\right] \quad \cdots\right) \tag{17}$$

Damping matrices have similar structure, while the dependence of Ω is omitted hereafter for the sake of brevity. This way, the fully assembled system of equations, without excitation, results:

$$[\mathbf{M}]\ddot{\mathbf{x}} + [\mathbf{C}]\dot{\mathbf{x}} + [\mathbf{K}]\mathbf{x} = 0 \tag{18}$$

with:

$$[\mathbf{M}] = \begin{bmatrix} [\mathbf{M}^{(r)}] & \mathbf{0} & \mathbf{0} \\ \mathbf{0} & [\mathbf{M}^{(f)}] & \mathbf{0} \\ \mathbf{0} & \mathbf{0} & [\mathbf{M}_{\mathrm{P}}] \end{bmatrix} \tag{19}$$

$$[\mathbf{C}] = \begin{bmatrix} [\mathbf{C}^{(r)}] + \Omega[\mathbf{G}^{(r)}] + [\mathbf{C}^{(rr)}] & -[\mathbf{C}^{(rf)}] & \mathbf{0} \\ -[\mathbf{C}^{(fr)}] & [\mathbf{C}^{(f)}] + [\mathbf{C}^{(ff)}] & \mathbf{0} \\ \mathbf{0} & \mathbf{0} & [\mathbf{C}_{\mathrm{P}}] \end{bmatrix} \tag{20}$$

$$[\mathbf{K}] = \begin{bmatrix} [\mathbf{K}^{(r)}] + [\mathbf{K}^{(rr)}] & -[\mathbf{K}^{(rf)}] & \mathbf{0} \\ -[\mathbf{K}^{(fr)}] & [\mathbf{K}^{(f)}] + [\mathbf{K}^{(ff)}] & \mathbf{0} \\ \mathbf{0} & \mathbf{0} & [\mathbf{K}_{\mathrm{P}}] \end{bmatrix} \tag{21}$$

Due to the layout of the test-rig in which the direction of the contact is mainly horizontal, the rub between the rotor and the seal strip occurs when the relative horizontal vibration between the node corresponding to the rub section and the housing exceeds the seal clearance δ. If this condition is verified, a force system is exchanged between the rotor and the stator, composed by:

- a normal component determined by the elastic reaction proportional to the penetration of the rotor in the sealing;

- a friction tangential reaction determined by Coloumb's law;
- the torques caused by the aforementioned forces on the rotor and on the housing.

In other terms:

$$\text{if } \left(y_{19}(t)-y_{\mathrm{P}}(t)\right)>\delta:$$

$$\mathbf{F}_c(t)=\left\{\cdots \underbrace{-\mu N \quad -N \quad 0 \quad 0 \quad -\mu N\frac{d_{m_{19}}}{2}}_{\text{node 19}} \cdots \underbrace{\mu N \quad N \quad 0 \quad 0 \quad 0 \quad \mu Na+Nb}_{\text{housing}}\right\}^{\mathrm{T}}, \tag{22}$$

$$N=k_c\left(y_{19}(t)-y_{\mathrm{P}}(t)-\delta\right)$$

The friction torque acting on the rotor has the effect to decelerate the rotor. Anyhow, the actual test-rig is driven by an electric motor that can hold a constant average rotating speed. Since the aim of the paper is not to accurately model the motor controller, its effect on the rotor is simply modelled by means of a motor torque acting on the first rotor node that balances the effect of the friction torque, when the contact happens:

$$\text{if } \left(y_{19}(t)-y_{\mathrm{P}}(t)\right)>\delta:$$

$$\mathbf{M}(t)=\left\{\underbrace{0 \quad 0 \quad 0 \quad 0 \quad \mu N\frac{d_{m_{19}}}{2}}_{\text{node 1}} \cdots\right\}^{\mathrm{T}} \tag{23}$$

The remaining external forcing systems acting on the rotor are the weight $\mathbf{W}$ and the residual unavoidable unbalance distribution which is modelled by means of a lumped external force in correspondence of the second inertia disk (node 15):

$$\mathbf{F}_{unb}(t)=\left\{\cdots \underbrace{m e\Omega^2\cos\left(\Omega t+\varphi_{unb}\right) \quad m e\Omega^2\sin\left(\Omega t+\varphi_{unb}\right) \quad 0 \quad 0 \quad 0\cdots}_{\text{node 15}}\right\}^{\mathrm{T}} \tag{24}$$

By considering all the excitations, the fully assembled system of equations is non-linear due to the rub effect and results:

$$[\mathbf{M}]\ddot{\mathbf{x}}+[\mathbf{C}]\dot{\mathbf{x}}+[\mathbf{K}]\mathbf{x}=\mathbf{F}_c(t)+\mathbf{M}(t)+\mathbf{F}_{unb}(t)+\mathbf{W}=\mathbf{F}(t)+\mathbf{W} \tag{25}$$

The non-linear system of equations in eq. (27) is integrated in the time domain using the Newmark's implicit method, in which the forcing vector $\mathbf{F}(t)$ is recalculated at each time step in order to evaluate if rub happens. The algorithm is the following:

1. Starting from a suitable set of initial conditions $\mathbf{x}_0$ and $\dot{\mathbf{x}}_0$ for $t=0$, which actually correspond to a point on the steady state orbit without rub for the rotor nodes and null displacements and velocities for the housing, the force vector $\mathbf{F}(0)$ is calculated, using eqs. (22)-(24).
2. The initial acceleration vector is calculated by:

$$\ddot{\mathbf{x}}_0=[\mathbf{M}]^{-1}\left(\mathbf{F}(0)+\mathbf{W}-[\mathbf{C}]\dot{\mathbf{x}}_0-[\mathbf{K}]\mathbf{x}_0\right) \tag{26}$$

3. Starting from the first time step, in a general time step *i*-th, the new force vector $\mathbf{F}(t_i)$ is calculated and the generalized displacements, accelerations and velocities are equal to:

$$\mathbf{x}_i=\left[\frac{1}{\bar{a}\,\Delta t^2}[\mathbf{M}]+\frac{\bar{b}}{\bar{a}\,\Delta t}[\mathbf{C}]+[\mathbf{K}]\right]^{-1}\left(\begin{array}{l}\mathbf{F}(t_i)+\mathbf{W}+\left[\frac{1}{\bar{a}\,\Delta t^2}[\mathbf{M}]+\frac{\bar{b}}{\bar{a}\,\Delta t}[\mathbf{C}]\right]\mathbf{x}_{i-1}+\\ +\left[\frac{1}{\bar{a}\,\Delta t}[\mathbf{M}]-\left(1-\frac{\bar{b}}{\bar{a}}\right)[\mathbf{C}]\right]\dot{\mathbf{x}}_{i-1}+\\ +\left[\frac{1}{\bar{a}}\left(\frac{1}{2}-\bar{a}\right)[\mathbf{M}]-\Delta t\left(1-\frac{\bar{b}}{2\bar{a}}\right)[\mathbf{C}]\right]\ddot{\mathbf{x}}_{i-1}\end{array}\right) \tag{27}$$

$$\ddot{\mathbf{x}}_i=\frac{1}{\bar{a}\,\Delta t^2}\left(\mathbf{x}_i-\mathbf{x}_{i-1}-\dot{\mathbf{x}}_{i-1}\Delta t\right)-\frac{1}{\bar{a}}\left(\frac{1}{2}-\bar{a}\right)\ddot{\mathbf{x}}_{i-1} \tag{28}$$

$$\dot{\mathbf{x}}_i = \frac{\bar{b}}{\bar{a}\,\Delta t}\left(\mathbf{x}_i - \mathbf{x}_{i-1}\right) + \left(1 - \frac{\bar{b}}{\bar{a}}\right)\dot{\mathbf{x}}_{i-1} + \Delta t\left(1 - \frac{\bar{b}}{2\,\bar{a}}\right)\ddot{\mathbf{x}}_{i-1} \tag{29}$$

The constants $\bar{a}$ and $\bar{b}$ of the Newmark's method are assumed respectively equal to 0.25 and 0.5; this is equivalent to the "trapezium rule" and assures that the implicit integration is unconditionally stable, without adding numerical spurious damping (high values of $\bar{b}$). In fact it can be proven that Newmark's method is unconditionally stable if $\bar{b} \geq 0.5$ and $\bar{a} \geq 0.25(0.5+\bar{b})^2$.

SIMULATION RESULTS

Some simulations have been made using the proposed method and implementing the model of the test-rig. Since in the actual layout the supporting structure is rigid in the speed range of analysis, the foundation d.o.f.s are neglected in the calculation. Three different cases have been simulated in order to evaluate the differences in the dynamical behaviour when the test-rig is operating below, close or over the first lateral critical speed. From the Bode diagram of the system response without rub (Figure 3) it is possible to see that, due to the system anisotropy, horizontal and vertical critical speeds are actually split. Anyhow it will be decided to consider as critical speed that of 1090 rpm, due to the high dynamical amplification, even only in vertical direction. Also the torsional eigenfrequencies have been evaluated before the simulation. The three first ones resulted 132.48, 545.64 and 1180.63 Hz.

All the simulations have been made by using a time step of 1e–4 s and considering the duration of 10 s. The friction coefficient μ has been considered equal to 0.3. The damped natural frequencies of the obstacle (when not in contact with shaft) have been set equal to 25.41, 43.01, 51.41, 70.73 (twice) and 74.22 Hz. The rotor is loaded by its own weight and by an unbalance of 1e–4 kg m which is set to bring the shaft in contact with the seal.

Dynamical behaviour below the critical speed (700 rpm)

At low speeds, in rubbing conditions, the size of the shaft orbits in the bearings (Figure 4 and Figure 5) and in the rubbing node (Figure 6) are reduced with respect to the non rubbing condition, and present some irregularity in its shape in the angular positions where the rub occurs.

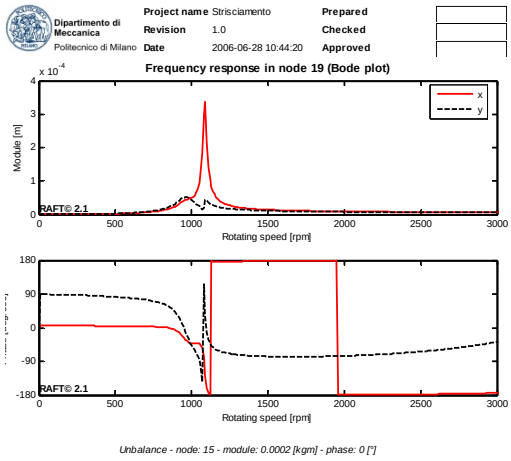

Figure 3. Bode diagram in the rubbing section due to the considered unbalance, w/o rub.

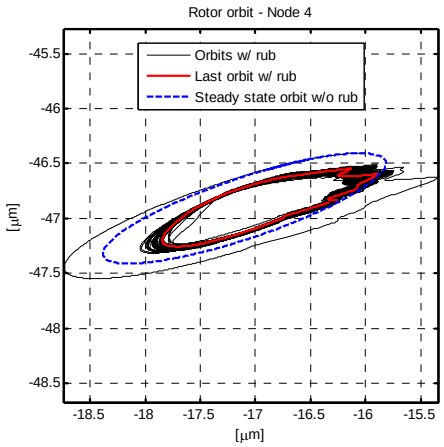

Figure 4. Rotor orbits, brg. #1, rotating speed 700 rpm.

Also some random noise is superposed to the steady state "mean" orbit. The spectra of the vertical and horizontal shaft vibrations also show some higher harmonic components (2X, 3X and so on) and some noise in a higher frequency range (60-100 Hz), as can be seen in Figure 7 for bearing 2 location. Higher harmonics and noise on the orbits are due to rubbing and are absent when contact does not exist.

The normal contact force shown in Figure 8 is intermittent: during the theoretical rubbing arc, in which contact can occur, contact occurs randomly between 2 and 4 times, and also its duration varies randomly between two extreme values. Surprisingly the maximum contact force is almost constant. The spectrum of the contact force (Figure 9) shows a rather rich content in the higher frequency range (150-250 Hz). The intermittent normal contact force, and consequently also the tangential friction force, excite both the vibrations of the obstacle and the torsional vibration of the shaft. The spectrum of the horizontal component of the vibration of the obstacle is shown in Figure 10, while the RMS value is 0.1415 μm. On real machines, accelerometers could be used to measure casing vibrations, therefore the RMS values of the acceleration would be much higher due to the higher frequency content of the vibration. These

values could certainly be measured. Several harmonics of the rotating speed frequency are excited but also some noise appears in the frequency range of the natural frequencies of the obstacle.

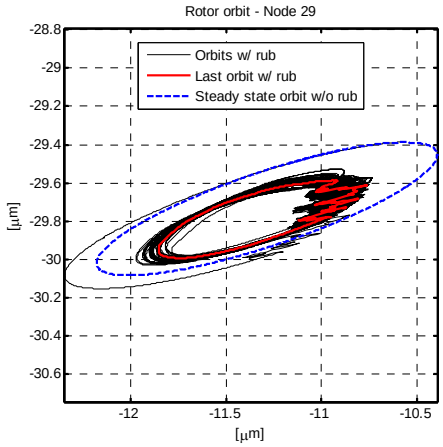

Figure 5. Rotor orbits, brg. #2, rotating speed 700 rpm.

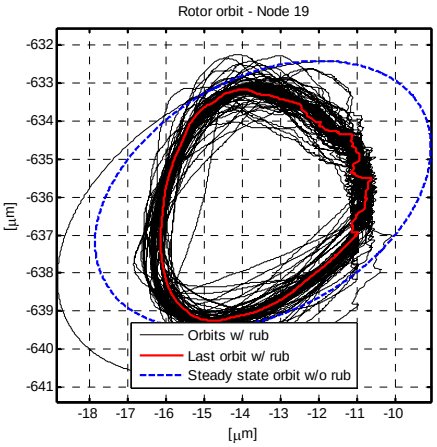

Figure 6. Rotor orbits, rubbing node, rotating speed 700 rpm.

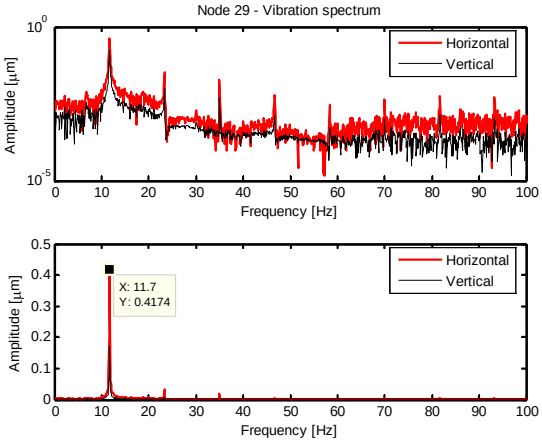

Figure 7. Shaft vibration spectra, brg. #2, rotating speed 700 rpm (low frequency range).

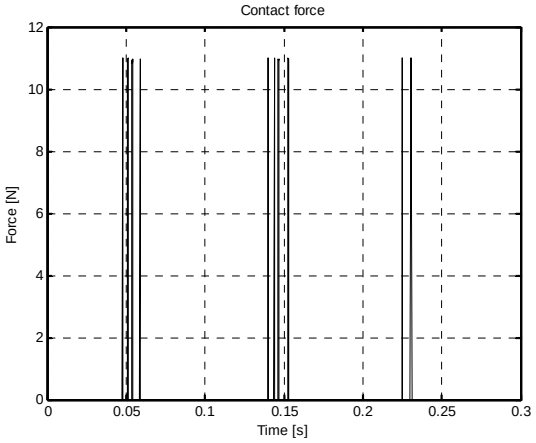

Figure 8. Close up of the normal contact force, rotating speed 700 rpm.

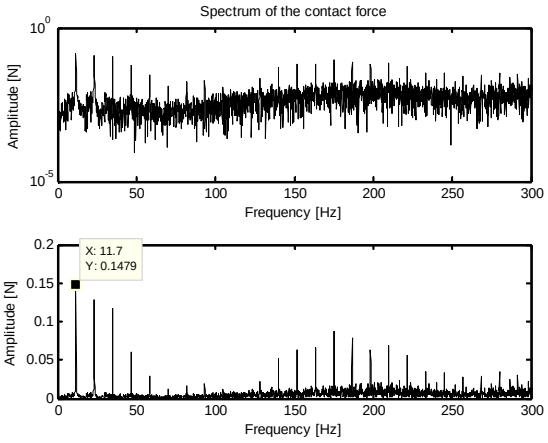

Figure 9. Normal contact force spectrum, rotating speed 700 rpm (low frequency range).

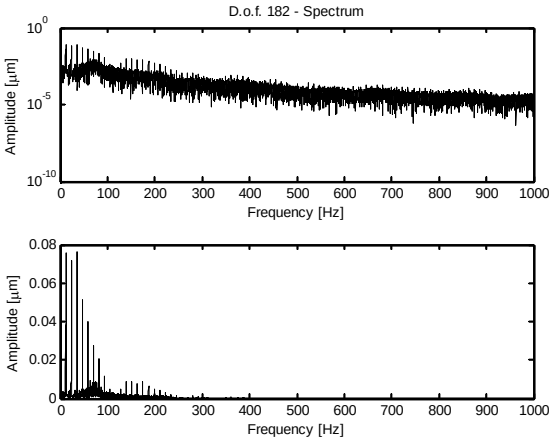

Figure 10. Spectrum of the horizontal displacement of the obstacle, rotating speed 700 rpm (high frequency range).

The torsional vibration spectrum (Figure 11) shows a strong excitation of the first 3 natural torsional frequencies and the RMS value is 1.7270 μrad.

Several symptoms seem to be available for detecting a rubbing condition:

- orbit distortion in the bearings which could be measured by the standard proximity probes of industrial turbomachinery;
- the change in vibrations of the stationary casing of the machine, although rather small could be detected by accelerometers placed on the casing;
- torsional vibrations, which normally are not measured in industrial machines, could represent an additional symptom.

All these results need to be validated by experimental results obtained on a laboratory test-rig or better on a real machine. Since the flexural natural frequencies of the shaft on its bearings and supports are representative of a full size steam turbine, from dynamical point of view the 2 systems are similar

The possibility that these results could be transferred to big sized industrial machines depends then on the scaling factor of contact forces and inertia.

Regarding the shaft orbit distortion in correspondence of the bearings, the sensitivity to rubbing contact force can be roughly estimated considering the ratio of contact force to static bearing load: this ratio is around 0.05 for the model of the test rig. Similar values could be suitable for real full size machines.

Regarding the casing vibrations not only a scaling factor must be considered, but the dynamical behaviour of the complete casing should be taken into account, also in the high frequency range.

Regarding the torsional vibrations, the rotary inertia of full size machines is much higher, the torsional critical speed are at lower frequencies, and its excitation depends also strongly on the location where rub is applied. Therefore it is difficult to predict the behaviour of full size machines.

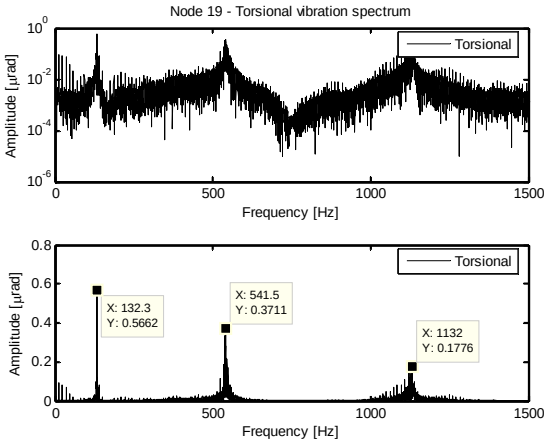

Figure 11. Torsional vibration spectrum, rubbing node, rotating speed 700 rpm.

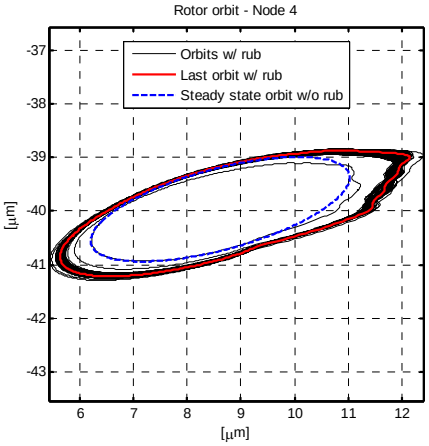

Figure 12. Rotor orbits, brg. #1, rotating speed 1500 rpm.

Dynamical behaviour over the critical speed (1500 rpm)

The size of the shaft orbits in the bearings in rubbing conditions (Figure 12 and Figure 13) are somewhat bigger with respect to the non-rubbing condition.

Distortion of shape is also remarkable. The contact force time history (Figure 14) is similar to the situation below the critical speed, its maximum value is lower (this depends on the actual interference conditions which are not controlled), its frequency content (Figure 15) is more rich in higher frequency components.

The excitation of the vibrations of the obstacle (Figure 16) and of the torsional vibrations (Figure 17) is stronger, with a respective RMS value of 0.7083 μm and 2.4921 μrad.

Dynamical behaviour close to the critical speed (1090 rpm)

Approaching the critical speed the behaviour changes from one revolution to the other and a quasi steady state situation is reached only after about 3 seconds (see e.g. the contact force time history of Figure 20). The orbits of the shaft in the bearings (Figure 18 and Figure 19) are highly enlarged and twisted, but are smooth with small irregularities. This could be attributed to the resonance effects which filters higher harmonic components.

The contact force (Figure 20) appears 1X and is continuous during rubbing (not intermittent), therefore the vibrations of the obstacle (Figure 21) and the torsional vibrations (Figure 22) are weakly excited in the higher frequency range. Their RMS is respectively 1.6087 μm and 1.7763 μrad.

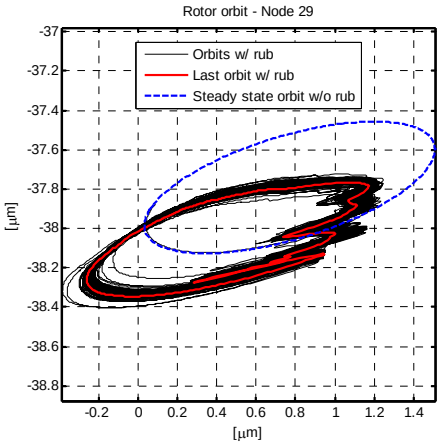

Figure 13. Rotor orbits, brg. #2, rotating speed 1500 rpm.

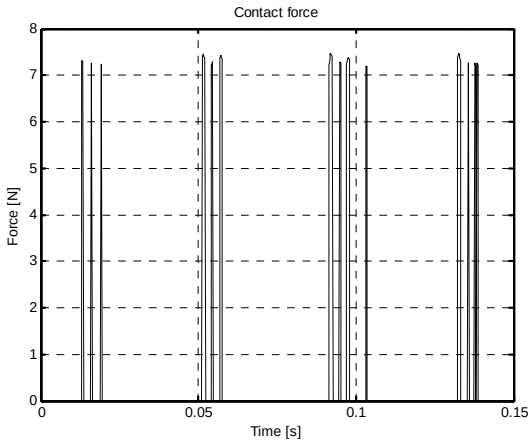

Figure 14. Close up of the normal contact force, rotating speed 1500 rpm.

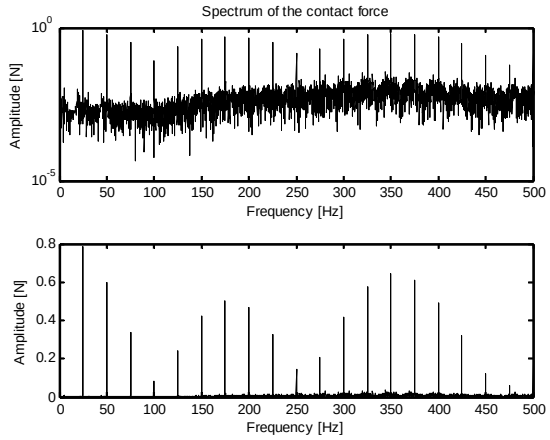

Figure 15. Normal contact force spectrum, rotating speed 1500 rpm (low frequency range).

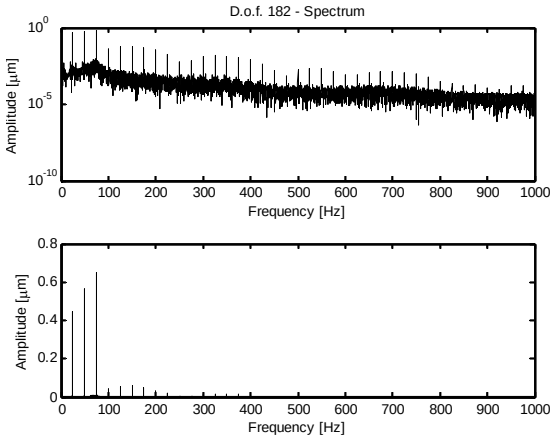

Figure 16. Spectrum of the horizontal displacement of the obstacle, rotating speed 1500 rpm (high frequency range).

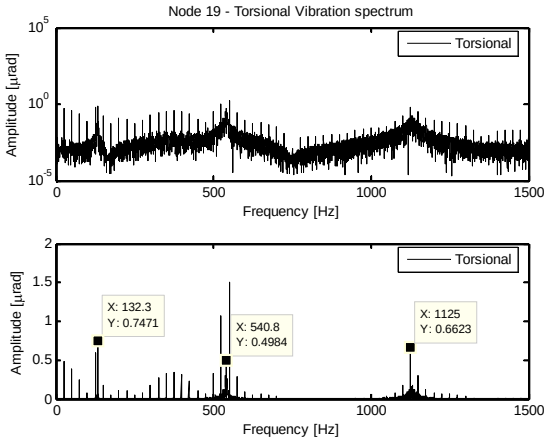

Figure 17. Torsional vibration spectrum, rubbing node, rotating speed 1500 rpm.

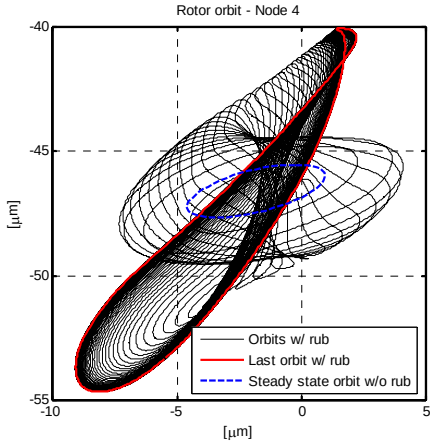

Figure 18. Rotor orbits, brg. #1, rotating speed 1090 rpm.

CONCLUSION

The simulation of the dynamical behaviour of the rubbing rotor shows that several different symptoms could be available to detect a rubbing condition, also if the rub is light. In particular, below the critical speed, the size of the shaft

orbits in the bearings, which normally correspond to the vibration measuring planes in real machines, are reduced with respect to the non-rubbing condition, with the same excitation. Conversely, over the critical speed the orbits are enlarged. In both cases, orbits are distorted and the spectra of the vertical and horizontal shaft vibrations show some higher harmonic components (2X, 3X and so on). Also the vibrations of the stationary casing of the machine present some variations, which could be detected by accelerometers placed on the casing, although rather small in amplitude. Finally, torsional vibrations at the natural torsional frequencies are excited. Unfortunately this important additional symptom is often not available in industrial machines, in which normally torsional vibrations are not measured.

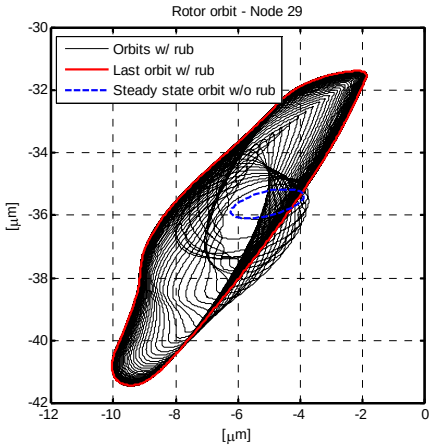

Figure 19. Rotor orbits, brg. #2, rotating speed 1090 rpm.

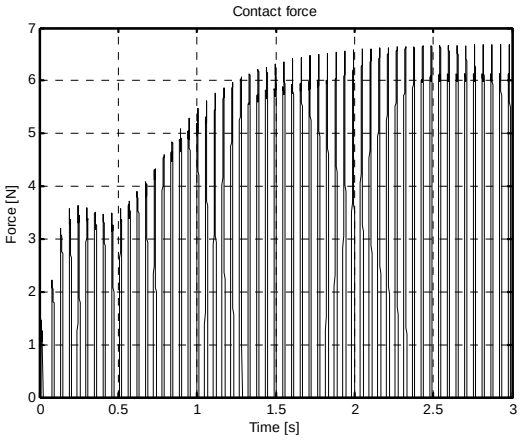

Figure 20. Close up of the normal contact force, rotating speed 1090 rpm.

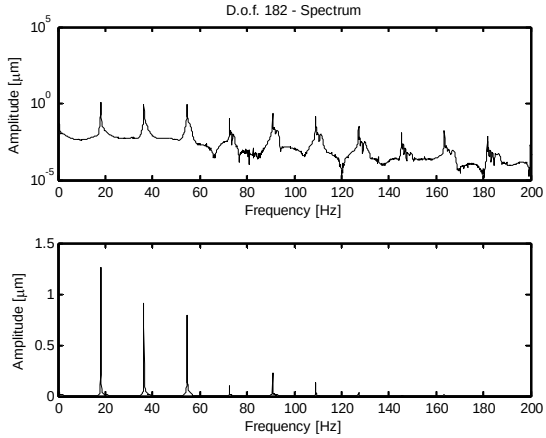

Figure 21. Spectrum of the hor. displacement of the obstacle, rotating speed 1090 rpm (low frequency range).

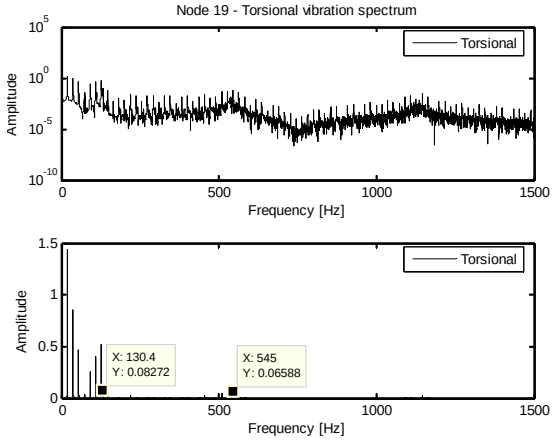

Figure 22. Torsional vibration spectrum, rubbing node, rotating speed 1090 rpm.

REFERENCES

Bachschmid, N., Pennacchi, P. and Venini, P., Spiral Vibrations in Rotors Due to a Rub, Proc. of IMechE-7th Int. Conf. on Vibrations in Rotating Machinery, 12-14 September 2000, University of Nottingham, UK, 249-258 (2000).

Bachschmid, N., Pennacchi, P. and Vania, A., Rotor-to-stator rub causing spiral vibrations: modelling and validation on experimental data of real rotating machine", IMechE paper C623/080/2004, Proc. of 8th International Conference on Vibrations in Rotating Machinery, 7-9 September 2004, Swansea, Wales, 671-680 (2004).

Childs, D., Turbomachinery Rotordynamics, John Wiley & Sons Inc, England, (1993).

Lalanne, M. and Ferraris, G., Rotordynamics Prediction in Engineering, John Wiley & Sons Inc, England, (1998).

Muszynska, A., Rotor to stationary element rub related vibration phenomena in rotating machinery – literature survey, Shock and Vibration Digest, 3-11 (1989).

Pennacchi, P., Bachschmid, N., Vania, A., Zanetta, G.A. and Gregori, L., Use of Modal Representation for the Supporting Structure in Model Based Fault Identification of Large Rotating Machinery: Part 1 – Theoretical Remarks, Mechanical Systems and Signal Processing, 20, No. 3, 662-681 (2006).

Stegemann, D., Reimche, W., Beermann, H. and Suedmersen, U., Analysis of short duration rubbing processes in steam turbines, VGB Kraftwerkstechnik, 73, n.10, 739-745 (1993).

RESPONSIBILITY NOTICE

The authors are the only responsible for the printed material included in this paper.